International Journal of Analysis and Applications

Perovskite Solar Cell Optimization via Polynomial Differential Quadrature Analysis with Block Marching

Waleed Mohammed Abdelfattah*

College of Engineering, University of Business and Technology, Jeddah 23435, Saudi Arabia

**Corresponding author:* w.abdelfattah@ubt.edu.sa

ABSTRACT. This paper introduces a novel numerical model for analyzing and optimizing the performance of perovskite solar cells, a technology with rapidly growing potential for high-efficiency energy conversion. The model focuses on a CH3NH3GeI3 absorber layer sandwiched between ZnO and PEDOT:PSS transport layers. It employs Poisson's and continuity equations, solved using the Polynomial Differential Quadrature (PDQ) method in conjunction with block marching and iterative techniques. This approach offers enhanced accuracy and computational efficiency compared to traditional methods, enabling more detailed device simulations. A MATLAB program is implemented to obtain numerical solutions, validated against experimental data and other numerical methods, demonstrating the model's reliability. A comprehensive parametric study is conducted to investigate the influence of critical parameters on the fill factor and efficiency of the solar cell. The results provide valuable, quantitatively precise insights for optimizing perovskite solar cell design, potentially accelerating the development of higher-performance, cost-effective solar energy solutions.

1. Introduction

The rapid progress in solar cell efficiency has sparked considerable research interest [1–5]. Transport layers, including hole transport layers (HTLs) and electron transport layers (ETLs), are essential components of solar cells. These layers not only facilitate efficient charge transport but also help to suppress recombination losses at interfaces [6–8]. Upon absorbing light, these layers generate electron-hole pairs, which are then transported to the respective electrodes through the HTL and ETL [9].

In past years, several researches were presented to investigate the efficiency of solar cells with perovskite layer (PSC) inserted between different layers such as ETL and HTL. The

Received Feb. 14, 2025

2020 Mathematics Subject Classification. 35Q60.

Key words and phrases. differential quadrature; block marching; iterative method; perovskite solar cells; fill factor; efficiency.

https://doi.org/10.28924/2291-8639-23-2025-98

ISSN: 2291-8639

influence of PSC efficiency by using different materials for ETL and HTL was investigated by Kanoun et al. [10]. ETL was employed to develop the efficiency of PSC with $MAPbI_3$ by Xu et al. [11]. Planar heterojunction perovskite cell based on ETL with SnO_2 material was presented numerically by Zhao et al. [12]. The structure of PSC planar heterojunction which consists of Spiro-OMeTAD as HTL and SnO_2 as ETL is studied by Kumar et al. [13]. Due to the advantages of PEDOT:PSS was introduced as HTL in p-i-n kind PSCs by Li et al. [14]. These merits are high exertion function, good film admission and good conductivity. But, PEDOT: PSS hurts some difficulties that decreases the stability because acidic and hygroscopic properties. The efficiency reached 15.24% by using PSC sandwiched with PEDOT:PSS material by Srivastava et al. [15]. The hysteresis property was reduced when Correa-Baena et al. [16] substituted the ETL material from Tio_2 to SnO_2 and increased the performance of PSC.

Several studies have investigated the performance of perovskite solar cells. Alam et al. [17] used SCAPS to simulate tin-based perovskite solar cells. Van Reenen et al. [18] employed finite difference methods to analyze current-voltage characteristics. Calado et al. [19] conducted experimental and numerical studies on transport layers and perovskite materials. Ravishankar et al. [20] analyzed surface polarization and device dynamics. Courtier et al. [21] compared finite element and finite difference methods for simulating charge transport. Zandi et al. [22] used finite element methods to model perovskite solar cells with ETL and HTL layers, achieving a simulated efficiency of 17.5%. These studies have provided valuable insights into the design and optimization of perovskite solar cells.

Ragb et al. [23] introduced several differential quadrature methods, namely PDQM, SDQM, DSCDQM-DLK, and DSCDQM-RSK, to analyze the behavior of perovskite solar cells. These methods were used to investigate the impact of interface materials on the efficiency and charge carrier dynamics of the devices. The results obtained suggest a potential efficiency of 32%. Various shape functions, including Cardinal sine, Lagrange interpolation, Regularized Shannon, and Delta Lagrange kernels, were considered. Among these, Lagrange interpolation polynomials were found to be particularly suitable for the numerical simulations [24,25].

This paper presents a numerical study of a perovskite solar cell model using the Polynomial Differential Quadrature (PDQ) method. The device consists of a halide perovskite absorber layer sandwiched between ZnO and PEDOT:PSS transport layers. The governing equations, derived from fundamental physical principles, are discretized using the PDQ method and solved iteratively [23,24,26]. A MATLAB script is developed to obtain numerical solutions, which are validated against experimental data and other numerical methods. A comprehensive parametric study is conducted to investigate the influence of various parameters, such as carrier mobilities, bandgap energy, layer thickness, temperature, wavelength, and doping concentrations, on the fill factor and efficiency of the solar cell. The

results of this study provide valuable insights for optimizing the design and performance of perovskite solar cells.

2. THE PROBLEM FORMULATION

A solar cell model consists of halide perovskite CH3NH3GeI3 as absorber layer inserted between ETL (ZnO) and HTL (PEDOT:PSS) [2,17–22,27].

Based on drift and diffusion equations, the governing equations are described as follow [17,18,27]:

$$\frac{\partial H}{\partial t}+\frac{1}{q}\frac{\partial J_H}{\partial x}=F_{photon}\times\alpha\times e^{(-\alpha x)}-\frac{E\times H}{\tau_{Hole}E+\tau_{Electron}H}, \tag{1}$$

$$\frac{\partial E}{\partial t}-\frac{1}{q}\frac{\partial J_E}{\partial x}=F_{photon}\times\alpha\times e^{(-\alpha x)}-\frac{E\times H}{\tau_{Hole}E+\tau_{Electron}H}, \tag{2}$$

$$J_H=-qD_{Hole}\left(\frac{\partial H}{\partial x}+\frac{H}{V_{th}}\frac{\partial \Phi}{\partial x}\right), \tag{3}$$

$$J_E=qD_{Electron}\left(\frac{\partial E}{\partial x}-\frac{E}{V_{th}}\frac{\partial \Phi}{\partial x}\right), \tag{4}$$

where H and E represent the hole and electron densities, respectively. J_H and J_E denote the hole and electron current densities, respectively. q is the elementary charge. D_{Hole} and $D_{Electron}$ are the hole and electron diffusion coefficients, respectively. V_T is the thermal voltage. F_{photon} is the incident photon flux, and α is the absorption coefficient. $\tau_{Electron}$ and τ_{Hole} are electron and hole lifetimes.

The electrostatic potential (Φ) can be calculated by Poisson formulation as follow [2,17–22,27]:

$$\frac{\partial^2\Phi}{\partial x^2}=\frac{q}{\varepsilon}(H-E) \tag{5}$$

where ε is the perovskite permittivity.

The boundary conditions for the unknowns ($E,\ H,\ J_E,\ J_H,\ \Phi$) can be described as [21,28]:

$$J_E(d)=0,\quad J_H(0)=0, \tag{6}$$

$$E(0) = N_C\, e^{-\frac{E_c - E_{fn}}{kT}}, \quad H(d) = N_v\, e^{\frac{E_v - E_{fh}}{kT}} \tag{7}$$

$$\Phi(0) = \frac{E_{fn} - E_{fh}}{d}, \qquad \Phi(d) = \frac{E_{fn} - E_{fh}}{d}, \tag{8}$$

$$E(0) \times H(d) = N_c N_v\, e^{((E_{gap} - E_{fn} + E_{fh})/(-kT))} \tag{9}$$

where d represents the absorber layer thickness. E_{fn} and E_{fh} are the electron and hole quasi-Fermi levels, respectively. E_v and E_c are valence and conduction gap energy, respectively. N_C and Nv are effective density of states.

3. METHOD OF SOLUTION

This study introduces a novel approach based on the differential quadrature method, utilizing Lagrange interpolation polynomials, to model a perovskite absorber layer sandwiched between ETL and HTL layers. This approach builds upon the work of previous researchers [2,17–22,27].

The anonymous ξ and the derivatives are the calculation weighted linear sum of nodal results, ξ_i as [24,25]:

$$\xi(x_i) = \sum_{j=1}^{N} \left[\frac{1}{x_i - x_j} \left(\frac{\prod_{k=1}^{N} (x_i - x_k)}{\prod_{j=1,\, j\neq k}^{N} (x_j - x_k)} \right) \right] \times \xi(x_j), \qquad \text{where} \quad i = 1, 2, \ldots N \tag{10}$$

$$\left. \frac{\partial^r \xi}{\partial x^r} \right|_{x = x_i} = \sum_{j=1}^{N} \Gamma_{ij}^{(r)}\, \xi(x_j), \qquad \text{where} \quad i = 1, 2, \ldots N, \quad \xi(E,\, H,\, \Phi) \tag{11}$$

where N represents the grid points. $\Gamma_{ij}^{(r)}$ represents the weighting coefficient of r^{th} derivatives and can be determined as [24,25]:

$$\Gamma_{ij}^{(1)} = \begin{cases} \dfrac{1}{(x_i - x_j)} \prod_{k=1,\, k\neq i,j}^{N} \dfrac{(x_i - x_k)}{(x_j - x_k)} & i \neq j \\ -\sum_{j=1,\, j\neq i}^{N} \Gamma_{ij}^{(1)} & i = j \end{cases}, \quad \left[\Gamma_{ij}^{(r)}\right] = \left[\Gamma_{ij}^{(1)}\right] \left[\Gamma_{ij}^{(r-1)}\right], (r = 2, 3, \ldots) \tag{12}$$

To reach high accurate value for PDQM, Gauss-Chebyshev-Lobatto discretization are used to contribute non-uniform grid points for resolving the governing equations as follow [24,25]:

$$x_i = \frac{1}{2}\left[1-\cos\left(\frac{i-1}{N-1}\pi\right)\right],\ (i=1,2,...N) \tag{13}$$

Substitution from (7-10) into (1-5), the governing equations can be presented as:
Firstly, we solve the governing equations for this model at steady state:

$$-qD_{Hole}\left(\sum_{j=1}^{N}\Gamma_{ij}^{(2)}H+\frac{1}{V_{th}}\left(\sum_{k=1}^{N}\delta_{ik}H_k\times\sum_{j=1}^{N}\Gamma_{ij}^{(2)}\Phi_j+\sum_{j=1}^{N}\Gamma_{ik}^{(1)}\Phi_k\times\sum_{j=1}^{N}\Gamma_{ij}^{(1)}H_j\right)\right)=$$
$$q\times\left(F_{photon}\times\alpha\times e^{(-\alpha x)}-\frac{\sum_{k=1}^{N}\delta_{ik}E_k\sum_{j=1}^{N}\delta_{ij}H_j}{\tau_H\sum_{k=1}^{N}\delta_{ik}E_k+\tau_E\sum_{j=1}^{N}\delta_{ij}H_j}\right), \tag{14}$$

$$qD_{Electron}\left(\sum_{j=1}^{N}\Gamma_{ij}^{(2)}E-\frac{1}{V_{th}}\left(\sum_{k=1}^{N}\delta_{ik}E_k\times\sum_{j=1}^{N}\Gamma_{ij}^{(2)}\Phi_j+\sum_{j=1}^{N}\Gamma_{ik}^{(1)}\Phi_k\times\sum_{j=1}^{N}\Gamma_{ij}^{(1)}E_j\right)\right)=$$
$$-q\times\left(F_{photon}\times\alpha\times e^{(-\alpha x)}-\frac{\sum_{k=1}^{N}\delta_{ik}E_k\sum_{j=1}^{N}\delta_{ij}H_j}{\tau_H\sum_{k=1}^{N}\delta_{ik}E_k+\tau_E\sum_{j=1}^{N}\delta_{ij}H_j}\right), \tag{15}$$

$$\sum_{j=1}^{N}\Gamma_{ij}^{(2)}\Phi_j+\frac{q}{\varepsilon}\sum_{j=1}^{N}\delta_{ij}E_j-\frac{q}{\varepsilon}\sum_{j=1}^{N}\delta_{ij}H_j=0, \tag{16}$$

The boundary conditions is augmented in the steady state governing equations (14-16). Therefore, the initial values for E, H, J_E, J_H, Φ ate obtained.

Next, we address the transient state of the system by solving the governing equations.

The block marching method is utilized to efficiently solve the time-dependent governing equations (1-5), as described in [23]. We assume that the distribution of grid point for all blocks is equal by setting ($\delta t=\delta t_1=\delta t_2=\delta t_3$ ...). The grid points in x and t directions can be written as [29]:

$$x_i=\left[L_x-L_x\times\cos\left(\frac{i-1}{N-1}\pi\right)\right]/2,\ (i=1:N) \tag{17}$$

$$t_k = \frac{\delta t}{2}\left[2K - 1 + \cos\left(\frac{k-1}{L-1}\pi\right)\right], \ (k = 1:L) \tag{18}$$

where N is the number of grid point in x direction, K is the number of block and L is the number of time level in the block.

$$\sum_{j=1}^{L} \Gamma_{ij}^{-(1)} H_j + \frac{1}{q} \times \sum_{j=1}^{N} \Gamma_{ij}^{(1)} J_{H_j} = F_{photon} \times \alpha \times e^{(-\alpha x)} - \frac{\sum_{k=1}^{N} \delta_{ik} E_k \sum_{j=1}^{N} \delta_{ij} H_j}{\tau_H \sum_{k=1}^{N} \delta_{ik} E_k + \tau_E \sum_{j=1}^{N} \delta_{ij} H_j}, \tag{19}$$

$$\sum_{j=1}^{L} \Gamma_{ij}^{-(1)} E_j - \frac{1}{q} \times \sum_{j=1}^{N} \Gamma_{ij}^{(1)} J_{E_j} = F_{photon} \times \alpha \times e^{(-\alpha x)} - \frac{\sum_{k=1}^{N} \delta_{ik} E_k \sum_{j=1}^{N} \delta_{ij} H_j}{\tau_H \sum_{k=1}^{N} \delta_{ik} E_k + \tau_E \sum_{j=1}^{N} \delta_{ij} H_j}, \tag{20}$$

$$\sum_{j=1}^{N} \delta_{ij} J_{H_j} + qD_{Hole}\left(\sum_{j=1}^{N} \Gamma_{ij}^{(1)} H_j + \frac{1}{V_{th}} \sum_{k=1}^{N} \delta_{ik} H_k \sum_{j=1}^{N} \Gamma_{ij}^{(1)} \Phi_j\right) = 0, \tag{21}$$

$$\sum_{j=1}^{N} \delta_{ij} J_{E_j} - qD_{Electron}\left(\sum_{j=1}^{N} \Gamma_{ij}^{(1)} E_j - \frac{1}{V_{th}} \sum_{k=1}^{N} \delta_{ik} E_k \sum_{j=1}^{N} \Gamma_{ij}^{(1)} \Phi_j\right) = 0, \tag{22}$$

$$\sum_{j=1}^{N} \Gamma_{ij}^{(2)} \Phi_j + \frac{q}{\varepsilon} \sum_{j=1}^{N} \delta_{ij} E_j - \frac{q}{\varepsilon} \sum_{j=1}^{N} \delta_{ij} H_j = 0, \tag{23}$$

An iterative approach is utilized to solve the nonlinear system of equations that arise from the governing equations [23,24,26]. Initially, we solve the governing equations in both states as linear system. Then, we solve them as nonlinear system iteratively until achieving the required convergence [23,24,26] such:

$$\left|\frac{E_{m+1}}{E_m}\right| < 1, \qquad \left|\frac{H_{m+1}}{H_m}\right| < 1, \qquad \text{where } m = 0,\ 1,\ 2,\ \ldots$$

4. NUMERICAL RESULTS

The Polynomial Differential Quadrature (PDQ) method, utilizing Lagrange shape functions, was employed to analyze a perovskite solar cell model. The model consists of a CH3NH3GeI3 absorber layer sandwiched between electron transport layer (ETL) and hole

transport layer (HTL). The numerical results obtained using the PDQ method exhibit improved efficiency and convergence compared to previous studies with error of order 10^{-6}.

The materials properities are taken from earlier studies and scheduled in Table (1) as follow [2,17–22,27]:

Table 1 Key Parameters for Simulating Perovskite Solar Cell Components.

Symbol	V_{th} (V)	ε	q (C)	T(k)	D(nm)	B_n, B_p (ev)	ε_0 (F/m)	E_{gap} (V)	N_C , Nv (m^{-3})	D_H, D_E (m^2s^{-1})	α (m^{-1})
Value	$25.7x10^{-3}$	6.5	$1.6*10^{-19}$	298	250	0	$2.7*10^{-11}$	1.55	$1.8*10^{19}$	$1.7x10^{-4}$	$1.3x10^{7}$

A comprehensive comparison of the numerical results obtained using the proposed method with experimental data, exact solutions, and results from least-squares fitting, finite difference, and finite element methods is presented.

The value of fill factor (FF%) can be calculated the according to the following relation [15]:

$$FF\% = \frac{V_{max}\ J_{max}}{V_{oc}\ J_{sc}} \times 100 \tag{24}$$

The efficiency (χ) of the perovskite solar cell is determined using the following equation, as described in reference [15]:

$$\chi\% = \frac{V_{max}\ J_{max}}{J\ A} \times 100 = \frac{FF\% \times V_{oc}\ J_{sc}}{J\ A} \tag{25}$$

where J represents the solar intensity and A represents the area of the solar cell exposed to solar radiation.

Tables 2 and 3 present the impact of temperature on the efficiency of the PSC for both uniform and non-uniform mesh points. The results demonstrate that increasing the number of grid points leads to improved convergence of the numerical solution. The uniform grid points are defined by $[3,15]$, while the non-uniform grid points are defined by $[3,11]$ The obtained results are compared with experimental data [19], theoretical calculations [27], least-squares fitting [20], finite difference methods [18], and finite element methods [21,22]. Further, it's found from table 2 the number of grid points ≥ 15 for uniform PDQM at time of performance is 23.45 sec. Also, from table 3 it's observed the number of grid points is fewer ≥ 11 at time of performance is 15.35 sec for non-uniform PDQM. So, the presented method with non-uniform grid points is better than uniform grid points.

Table 2 The variance between efficiency (χ) by using uniform PDQM, different temperatures (k) and the results earlier techniques at various grid points (N).

$d = 250$ nm, τ_E =3 ns, τ_H =300 ns ,$D_{Electron} = 10^{-5} m^2 s^{-1}$, $D_{Hole} = 10^{-6}$ $m^2 s^{-1}$, $E_{gap} = 1.55eV$

Temperatures (k) / Grid point (N)	Efficiency (χ)					
	T_1 250	T_2 300	T_3 350	T_4 400	T_5 450	T_6 500
5	25.147	24.444	23.4789	21.1479	20.7390	19.6487
7	23.585	22.774	21.7842	20.0325	19.1879	16.2020
9	20.1874	19.1402	18.1010	17.7098	16.2021	15.1874
11	17.2105	16.1414	15.0349	14.2029	13.1785	12.2789
13	13.9874	12.9872	11.9871	10.9870	9.9869	8.9868
15	13.35	12.35	11.35	10.35	9.35	8.35
experiment results [19]	13.40	12.42	11.44	10.46	9.48	8.5
Theoretical results [27]	13.4	12.41	11.42	10.43	9.44	8.45
Least-squares fitting [20]	13.35	12.35	11.35	10.35	9.35	8.35
Finite difference [18]	13.35	12.35	11.35	10.35	9.35	8.35
Finite element [21,22]	13.35	12.35	11.35	10.35	9.35	8.35
Time of performance	23.45 sec. (Uniform mesh points ≥ 15)					

Table 3 The variance between efficiency (χ) by using Non- uniform PDQM, different temperatures (k) and the results earlier techniques at various grid points (N).

$d = 250$ nm, τ_E =3 ns, τ_H =300 ns ,$D_{Electron} = 10^{-5} m^2 s^{-1}$, $D_{Hole} = 10^{-6}$ $m^2 s^{-1}$, $E_{gap} = 1.55eV$

Temperatures (k) / Grid point (N)	Efficiency (χ)					
	T_1 250	T_2 300	T_3 350	T_4 400	T_5 450	T_6 500
3	23.784	22.3331	21.0045	20.7891	19.1478	18.7846
5	20.658	19.9874	18.4517	17.5478	16.4789	15.7896
7	17.1123	16.9874	15.1155	14.2781	13.0587	12.04789
9	14.2658	13.2677	12.2625	11.2754	10.2600	9.1588
11	13.35	12.35	11.35	10.35	9.35	8.35
experiment results [19]	13.40	12.42	11.44	10.46	9.48	8.5
Theoretical results [27]	13.4	12.41	11.42	10.43	9.44	8.45
Least-squares fitting [20]	13.35	12.35	11.35	10.35	9.35	8.35
Finite difference [18]	13.35	12.35	11.35	10.35	9.35	8.35
Finite element [21,22]	13.35	12.35	11.35	10.35	9.35	8.35
Time of performance	15.35 sec. (Non-uniform mesh points ≥ 11)					

Table 4 shows the effect of temperature on the fill factor of the PSC, considering different grid point distributions. Increasing the number of grid points leads to improved convergence of the numerical solution. The results obtained using the proposed method are in good agreement

with experimental data [19], theoretical calculations [27], least-squares fitting [20], finite difference methods [18], and finite element methods [21,22], particularly for non-uniform grid points. The proposed method achieves high accuracy with an error of 10^{-6}. A negative correlation is observed between efficiency and fill factor and temperature.

Table 4 The variance between fill factor (FF %) due to non-uniform PDQM, different temperatures (k) and the results earlier techniques at different grid points (N).

$d = 250$ nm, $\tau_E = 3$ ns, $\tau_H = 300$ ns, $D_{Electron} = 10^{-5} m^2 s^{-1}$, $D_{Hole} = 10^{-6}\ m^2 s^{-1}$, $E_{gap} = 1.55$eV

Temperatures (k) / Grid point (N)	Fill factor (FF %)					
	T_1 250	T_2 300	T_3 350	T_4 400	T_5 450	T_6 500
3	95.542	94.2489	93.0222	92.9123	91.5002	90.999
5	93.147	92.5478	91.0112	90.8745	89.5471	88.9512
7	90.001	89.2478	88.0001	87.2547	86.0145	85.9998
9	88.5891	86.5321	85.5624	84.5545	83.6621	82.5431
11	87.97	86.97	85.97	84.97	83.97	82.97
experiment results [19]	88	87	86	85	84	83
Theoretical results [27]	88.12	87.14	86.10	85.08	84.07	83.25
Least-squares fitting [20]	87.97	86.97	85.97	84.97	83.97	82.97
Finite difference [18]	87.97	86.97	85.97	84.97	83.97	82.97
Finite element [21,22]	87.97	86.97	85.97	84.97	83.97	82.97
Time of performance	15.35 sec. (Non-uniform mesh points ≥ 11)					

Table 5 demonstrate the variation of fill factor (FF %) and efficiency (χ) with time at $\Delta t = 0.5$ μs, $L = 12$. The obtained results are in good agreement with theoretical predictions [27] for a particular number of blocks ≥ 5 and a computational time of 17.87 seconds. So, decreasing time interval (Δt) hints to high effective for investigating the performance of Halide perovskite (CH3NH3GeI3) absorber layer inserted between electron ETL and HTL.

Table 5 Variation of fill factor (FF %) and efficiency (χ) with time using non-uniform PDQM at

$\Delta T = 0.5$ s, $L = 12$, $d = 250$ nm, $\tau_E = 3$ ns, $\tau_H = 300$ ns, $D_{Electron} = 10^{-5} m^2 s^{-1}$, $D_{Hole} = 10^{-6}\ m^2 s^{-1}$, $E_{gap} = 1.55$eV

No. of blocks / Time (s)	FF %				efficiency (χ)			
	1	3	5	Exact	1	3	5	Exact
0	90.83	90.54	90.25	90.25	10.874	9.881	9.723	9.723
50	90.54	90.28	90.14	90.14	15.888	14.947	14.847	14.847
100	90.24	90.05	89.85	89.85	15.779	14.952	14.914	14.914
150	90.01	89.85	89.25	89.25	15.992	14.974	14.925	14.925
200	89.88	89.25	88	88	16.222	14.987	14.874	14.874
250	89.59	89.06	87	87	16.225	14.995	14.885	14.885
300	89.22	88.75	86.45	86.45	16.229	14.999	14.890	14.890
350	88.99	88.5	85.55	85.55	16.257	15.001	14.905	14.905
400	88.75	88.25	85.5	85.5	16.112	15.005	14.918	14.918
Time of performance	17.87 (sec) -- over no. of blocks ≥ 5							

Figure 1 illustrates that increasing in temperature leads to decreasing fill factor percentage, and efficiency. Also, it displays that increasing in thickness of absorber layer (perovskite) leads to decreasing fill factor percentage, and increasing efficiency. So, the best conditions for obtaining high fill factor are absorber layer thickness equals to 200 nm and temperature equals to250 k, but for high efficiency absorber layer thickness should be more than 600 nm and temperature equal to250 k.

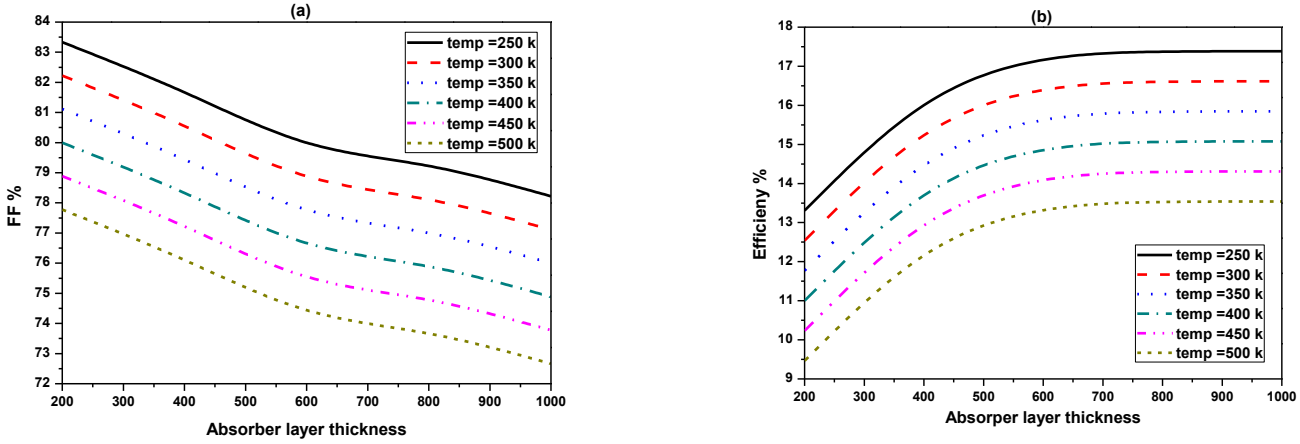

Fig. 1 The impact of temperature and absorber layer thickness on (a) Fill factor and (b) Efficiency

$E_{gap} = 1.55$ eV, $\tau_E = 3$ ns, $\tau_H = 300$ ns, $D_E = 10^{-5} m^2 s^{-1}$, $D_H = 10^{-6} m^2 s^{-1}$, $\mu_E = \mu_H = 2 \times 10^{-4} cm^2 / Vs$

Figure 2 demonstrates the effect of doping concentration and perovskite layer thickness on the key performance metrics of the PSC, namely fill factor and efficiency. This figure displays that the increasing in doping concentrations leads to increasing both FF % and χ % up to 10^{18} cm^{-3} then be constant after 10^{18} cm^{-3}.

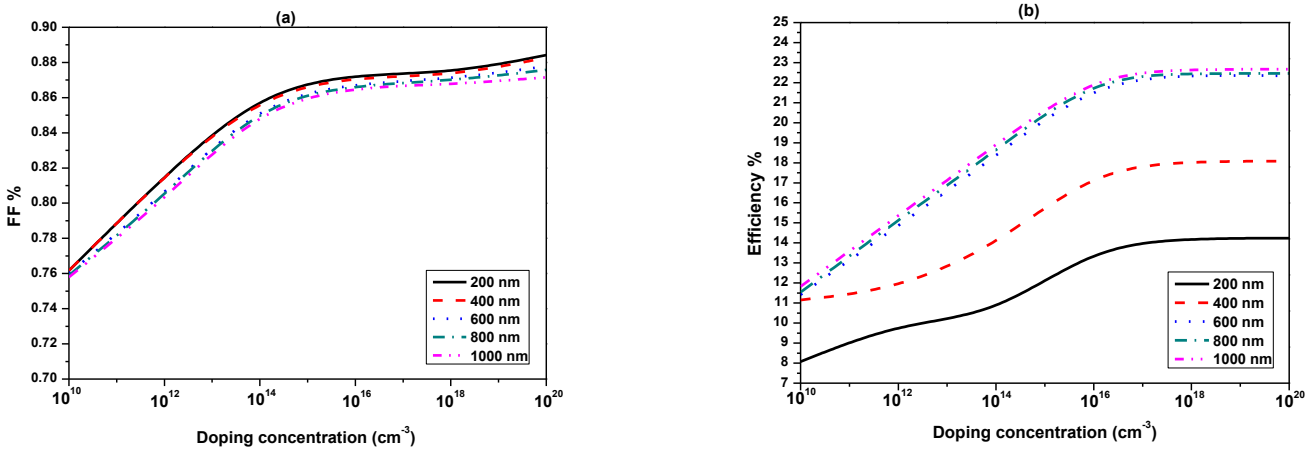

Fig. 2 The influence of varying doping concentrations and perovskite layer thicknesses on (a) Fill factor and (b) Efficiency of the PSC.

$E_{gap} = 1.55$ eV, $\tau_E = 3$ ns, $\tau_H = 300$ ns, $D_E = 10^{-5} m^2 s^{-1}$, $D_H = 10^{-6} m^2 s^{-1}$, $\mu_E = \mu_H = 2 \times 10^{-4} cm^2 / Vs$

Figure 3 demonstrates the effect of bandgap energy and carrier mobilities on the key performance metrics of the PSC, namely fill factor (FF %) and efficiency (χ %). The increase in energy gap reduces the fill factor and efficiency. The findings presented in Figure 3 highlight the positive correlation between carrier mobilities and device performance. A bandgap energy of 1.3 eV appears to be the optimal choice for maximizing fill factor and efficiency.

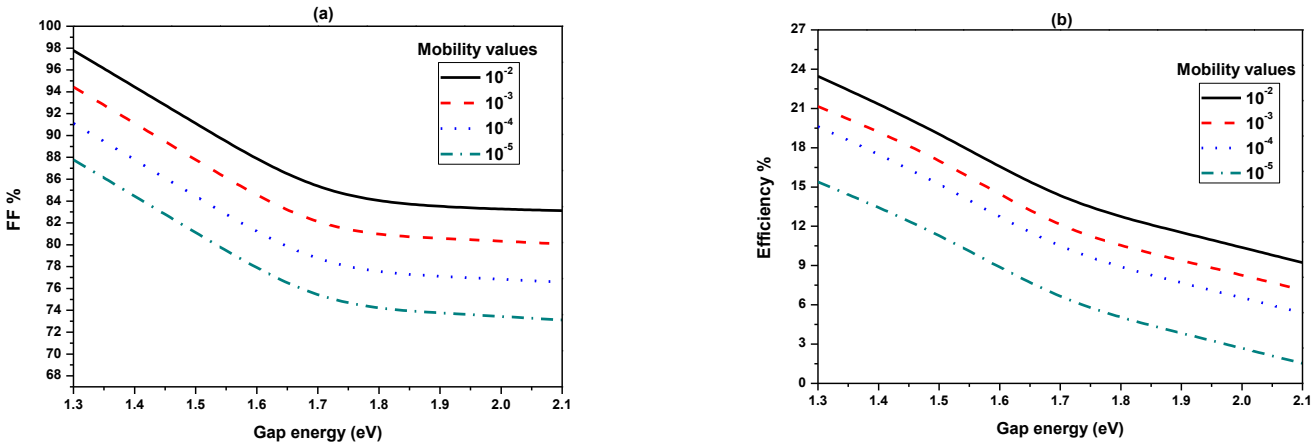

Fig. 3 The impact of bandgap energy and carrier mobilities on (a) Fill factor and (b) Efficiency.
$d = 250$ nm, τ_E =3 ns, τ_H =300 ns, $D_E = 10^{-5} m^2 s^{-1}$, $D_H = 10^{-6} m^2 s^{-1}$

Figure 4 illustrates the influence of wavelength (λ) and absorption factor (α) on the fill factor and efficiency of the PSC. The results indicate that increasing the wavelength up to 800 nm, coupled with a high absorption factor of 10^6 cm^{-1}, leads to improved device performance.

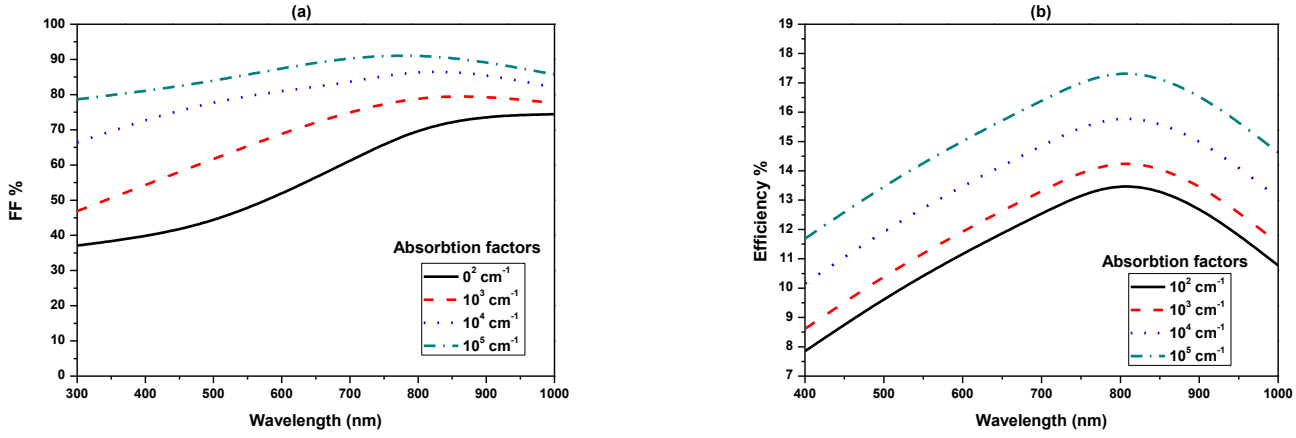

Fig. 4 The impact of wavelength (λ) and different absorption factors (α) on (a) Fill factor and (b) Efficiency.
$d = 250$ nm, $E_{gap} = 1.55$ eV, τ_E =3 ns, τ_H =300 ns, $D_E = 10^{-5} m^2 s^{-1}$, $D_H = 10^{-6} m^2 s^{-1}$, $\mu_E = \mu_H = 2 \times 10^{-4} cm^2 / Vs$

Figures (5-6) are performed at transient state where $\Delta T = 0.5$ s, L=12, and number of blocks =5. From all figures show that the fill factor has higher value at steady state than transient state, but the efficiency of PSC has higher value at transient state than steady state.

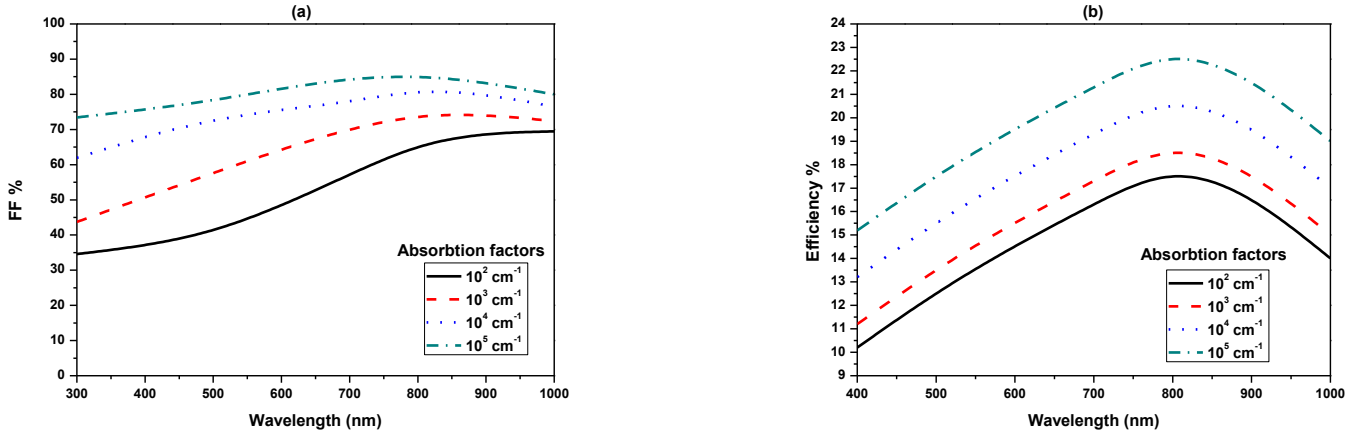

Fig. 5 The impact of wavelength (λ) and different absorption factors (α) on (a) Fill factor and (b) Efficiency at transient state.

$d = 400$ nm, $E_{gap} = 1.55$ eV, $\tau_E = 3$ ns, $\tau_H = 300$ ns, $D_E = 10^{-5} m^2 s^{-1}$, $D_H = 10^{-6} m^2 s^{-1}$, $\mu_E = \mu_H = 2 \times 10^{-4} cm^2 / Vs$

$\Delta T = 0.5$ s, L=12, and number of blocks $= 5$

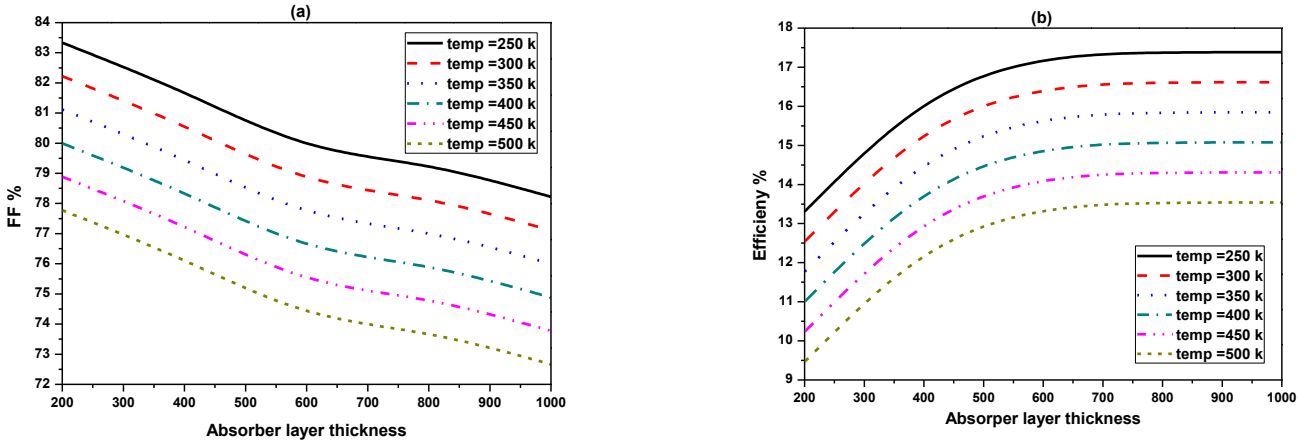

Fig. 6 The impact of different temperatures and absorber layer thickness on (a) Fill factor and (b) Efficiency at transient state. $\Delta T = 0.5$ s, L=12, and number of blocks $= 5$

5. Conclusion

The method of differential quadrature depended on the polynomial of Lagrange interpolation is employed for investigating a model of solar cell consisted of halide perovskite $CH_3NH_3GeI_3$ as absorber layer inserted between electron transport layer (ZnO) and hole transport layer (PEDOT:PSS). The PDQ method is utilized to linearize the nonlinear partial

differential equations, transforming them into a system of nonlinear algebraic equations that can be solved iteratively. Block marching technique is employed to solve transient problem. MATLAB script is performed to attain a solution for this problem. The attained results accept with previous experiment and finite difference scheme. The error of $\leq 10^{-6}$ are the advantages of this technique. The parametric analysis is familiarized to demonstrate the result of changing mobilities, gap energy, absorber thickness, temperatures, wavelength, and coefficient of absorption on efficiency and fill factor of solar cells. Consequently, the calculated results of this method are beneficial for enhancing the performance of perovskite solar cells. For all effects, it is found that:

- The best conditions for obtaining high fill factor (90%) are absorber layer thickness equals to 200 nm and temperature equals to250 k, but for high efficiency (23%) absorber layer thickness should be more than 600 nm and temperature equal to250 k.
- The increasing in doping concentrations leads to increasing both FF % and χ % up to 10^{18} cm^{-3} then is constant after 10^{18} cm^{-3}.
- A bandgap energy of 1.3 eV and mobilities of $\mu_E = \mu_H = 10^{-2} cm^2 / Vs$ are identified as the optimal choice for achieving superior fill factor and efficiency.
- The combination of wavelengths exceeding 800 nm and an absorption factor of 10^6 cm^{-1} yields the highest fill factor and power conversion efficiency.
- The fill factor has higher value (90%) at steady state than transient state (85%).
- The efficiency of PSC has higher value (23%) at transient state than steady state (18%).

The results obtained by PDQM helps to increase the efficiency of PSC. Recently, the industrials revolution depended on renewable energy, so PSC with high efficiency will lead to use it in many fields in the future. Therefore, in the future we will concern on changing material up to reaching higher efficiency in our researches.

Conflicts of Interest: The author declares that there are no conflicts of interest regarding the publication of this paper.

References

[1] H.J. Snaith, A. Abate, J.M. Ball, et al. Anomalous Hysteresis in Perovskite Solar Cells, J. Phys. Chem. Lett. 5 (2014), 1511–1515. https://doi.org/10.1021/jz500113x.

[2] F. Azri, A. Meftah, N. Sengouga, A. Meftah, Electron and Hole Transport Layers Optimization by Numerical Simulation of a Perovskite Solar Cell, Solar Energy 181 (2019), 372–378. https://doi.org/10.1016/j.solener.2019.02.017.

[3] A. Kojima, K. Teshima, Y. Shirai, T. Miyasaka, Organometal Halide Perovskites as Visible-Light Sensitizers for Photovoltaic Cells, J. Amer. Chem. Soc. 131 (2009), 6050–6051. https://doi.org/10.1021/ja809598r.

[4] D.Y. Son, S.G. Kim, J.Y. Seo, et al. Universal Approach toward Hysteresis-Free Perovskite Solar Cell via Defect Engineering, J. Amer. Chem. Soc. 140 (2018), 1358–1364. https://doi.org/10.1021/jacs.7b10430.

[5] M.A. Green, Y. Hishikawa, E.D. Dunlop, et al. Solar Cell Efficiency Tables (Version 51), Prog. Photovolt.: Res. Appl. 26 (2018), 3–12. https://doi.org/10.1002/pip.2978.

[6] H.S. Kim, C.R. Lee, J.H. Im, et al. Lead Iodide Perovskite Sensitized All-Solid-State Submicron Thin Film Mesoscopic Solar Cell with Efficiency Exceeding 9%, Sci. Rep. 2 (2012), 591. https://doi.org/10.1038/srep00591.

[7] A. Ahmed, K. Riaz, H. Mehmood, et al. Performance Optimization of CH3NH3Pb(I1-xBrx)3 Based Perovskite Solar Cells by Comparing Different ETL Materials through Conduction Band Offset Engineering, Opt. Mater. 105 (2020), 109897. https://doi.org/10.1016/j.optmat.2020.109897.

[8] Y.F. Makableh, G. Aljaiuossi, R. Al-Abed, Comprehensive Design Analysis of Electron Transmission Nanostructured Layers of Heterojunction Perovskite Solar Cells, Superlattices Microstruct. 130 (2019), 390–395. https://doi.org/10.1016/j.spmi.2019.05.017.

[9] V. Gonzalez-Pedro, E.J. Juarez-Perez, W.-S. Arsyad, E.M. Barea, F. Fabregat-Santiago, I. Mora-Sero, J. Bisquert, General Working Principles of CH3 NH3 PbX3 Perovskite Solar Cells, Nano Lett. 14 (2014), 888–893. https://doi.org/10.1021/nl404252e.

[10] A.A. Kanoun, M.B. Kanoun, A.E. Merad, S. Goumri-Said, Toward Development of High-Performance Perovskite Solar Cells Based on CH3NH3GeI3 Using Computational Approach, Solar Energy 182 (2019), 237–244. https://doi.org/10.1016/j.solener.2019.02.041.

[11] X. Xu, H. Zhang, J. Shi, et al. Highly Efficient Planar Perovskite Solar Cells with a TiO2 /ZnO Electron Transport Bilayer, J. Mater. Chem. A 3 (2015), 19288–19293. https://doi.org/10.1039/C5TA04239A.

[12] P. Zhao, Z. Lin, J. Wang, et al. Numerical Simulation of Planar Heterojunction Perovskite Solar Cells Based on SnO2 Electron Transport Layer, ACS Appl. Energy Mater. 2 (2019), 4504–4512. https://doi.org/10.1021/acsaem.9b00755.

[13] G. Kumar, J. Kaur, R. Basu, Performance Analysis of Planar Heterojunction Perovskite Solar Cell Featuring Double Hole Transport Layer & Backplane, Silicon 14 (2022), 463–474. https://doi.org/10.1007/s12633-020-00820-8.

[14] E. Li, W. Li, L. Li, et al. Efficient p-i-n Structured Perovskite Solar Cells Employing Low-Cost and Highly Reproducible Oligomers as Hole Transporting Materials, Sci. China Chem. 62 (2019), 767–774. https://doi.org/10.1007/s11426-018-9452-9.

[15] M. Srivastava, K. Surana, S. Singh, et al. Highly Efficient Sandwich Structured Perovskite Solar Cell Using PEDOT:PSS in Room Ambient Conditions, Mater. Today: Proc. 34 (2021), 675–678. https://doi.org/10.1016/j.matpr.2020.03.329.

[16] J.P. Correa Baena, L. Steier, W. Tress, et al. Highly Efficient Planar Perovskite Solar Cells through Band Alignment Engineering, Energy Environ. Sci. 8 (2015), 2928–2934. https://doi.org/10.1039/C5EE02608C.

[17] I. Alam, M.A. Ashraf, Effect of Different Device Parameters on Tin-Based Perovskite Solar Cell Coupled with In2 S3 Electron Transport Layer and CuSCN and Spiro-OMeTAD Alternative Hole Transport Layers for High-Efficiency Performance, Energy Sources Part A 46 (2024), 17080–17096. https://doi.org/10.1080/15567036.2020.1820628.

[18] S. Van Reenen, M. Kemerink, H.J. Snaith, Modeling Anomalous Hysteresis in Perovskite Solar Cells, J. Phys. Chem. Lett. 6 (2015), 3808–3814. https://doi.org/10.1021/acs.jpclett.5b01645.

[19] P. Calado, A.M. Telford, D. Bryant, et al. Evidence for Ion Migration in Hybrid Perovskite Solar Cells with Minimal Hysteresis, Nat. Commun. 7 (2016), 13831. https://doi.org/10.1038/ncomms13831.

[20] S. Ravishankar, O. Almora, C. Echeverría-Arrondo, et al. Surface Polarization Model for the Dynamic Hysteresis of Perovskite Solar Cells, J. Phys. Chem. Lett. 8 (2017), 915–921. https://doi.org/10.1021/acs.jpclett.7b00045.

[21] N.E. Courtier, G. Richardson, J.M. Foster, A Fast and Robust Numerical Scheme for Solving Models of Charge Carrier Transport and Ion Vacancy Motion in Perovskite Solar Cells, Appl. Math. Model. 63 (2018), 329–348. https://doi.org/10.1016/j.apm.2018.06.051.

[22] S. Zandi, M. Razaghi, Finite Element Simulation of Perovskite Solar Cell: A Study on Efficiency Improvement Based on Structural and Material Modification, Solar Energy 179 (2019), 298–306. https://doi.org/10.1016/j.solener.2018.12.032.

[23] O. Ragb, M. Mohamed, M.S. Matbuly, O. Civalek, An Accurate Numerical Approach for Studying Perovskite Solar Cells, Int. J. Energy Res. 45 (2021), 16456–16477. https://doi.org/10.1002/er.6892.

[24] O. Ragb, M. Mohamed, M.S. Matbuly, Vibration Analysis of Magneto-Electro-Thermo NanoBeam Resting on Nonlinear Elastic Foundation Using Sinc and Discrete Singular Convolution Differential Quadrature Method, Mod. Appl. Sci. 13 (2019), 49. https://doi.org/10.5539/mas.v13n7p49.

[25] C. Shu, Differential Quadrature and Its Application in Engineering, Springer, 2012. https://doi.org/10.1007/978-1-4471-0407-0.

[26] O. Ragb, M. Mohamed, M.S. Matbuly, Free Vibration of a Piezoelectric Nanobeam Resting on Nonlinear Winkler-Pasternak Foundation by Quadrature Methods, Heliyon 5 (2019), e01856. https://doi.org/10.1016/j.heliyon.2019.e01856.

[27] S.Z. Haider, H. Anwar, S. Manzoor, A.G. Ismail, M. Wang, A Theoretical Study for High-Performance Inverted p-i-n Architecture Perovskite Solar Cells with Cuprous Iodide as Hole Transport Material, Curr. Appl. Phys. 20 (2020), 1080–1089. https://doi.org/10.1016/j.cap.2020.06.022.

[28] J.A. Nelson, The Physics of Solar Cells, World Scientific, 2003. https://doi.org/10.1142/p276.

[29] C. Shu, Q. Yao, K.S. Yeo, Block-Marching in Time with DQ Discretization: An Efficient Method for Time-Dependent Problems, Comput. Methods Appl. Mech. Eng. 191 (2002), 4587–4597. https://doi.org/10.1016/S0045-7825(02)00387-0.